ELSEVIER

Materials Science and Engineering A 382 (2004) 162–170

MATERIALS SCIENCE & ENGINEERING A

www.elsevier.com/locate/msea

The mechanical response of an A359/SiC_p MMC and the A359 aluminum matrix to dynamic shearing deformations

Yulong Li [a,1], K.T. Ramesh [a,*], E.S.C. Chin [b]

[a] *Department of Mechanical Engineering, The Johns Hopkins University, Baltimore, MD 21218, USA*
[b] *Army Research Laboratory, Weapons and Materials Research Directorate, Aberdeen Proving Ground, MD 21005, USA*

Received 26 January 2004; received in revised form 17 April 2004

Abstract

The mechanical response of a metal–matrix composite to dynamic shearing deformations has been measured, using a new design of the thin-walled tubular specimen for the torsional Kolsky bar experiment that allows working with these difficult-to-machine materials. The advantages of using the new specimen design are as follows: (i) the thickness of the thin wall along the axial direction is very uniform; (ii) specimen machining is extremely simple; (iii) the cost of specimen machining is greatly reduced. The approach has been used to characterize the high shear strain rate ($10^3\ s^{-1}$) behavior of an A359/SiC_p composite and its corresponding A359 monolithic alloy with the torsion Kolsky bar. The experimental results show that the flow stress of the composite in shear increases in the presence of SiC particles, whereas the failure strain is reduced. The shear failure strains of both the A359/SiC_p composite and the A359 monolithic alloy appear to increase with increasing strain rate. Previous observations have shown that particle fracture develops during compressive deformations of this material. However, particle fracture is not a significant damage mode during the shearing deformations of the composite, and this is reflected in differences between the torsional and tension behaviors of the material.

Keywords: Metal–matrix composites; Torsion; High-strain-rate; Shearing; Failure; Rate-dependence

1. Introduction

Ceramic particle-reinforced metal–matrix composites are candidate materials for advanced structural armors. Bless et al. [1] have observed that composites of 6061-T6 and 2014-T6 aluminum alloys reinforced by SiC particles were as much as three times more efficient than the unreinforced aluminum alloys in defeating tungsten projectiles at 1.2 km/s. Similarly, Vaziri et al. [2] performed ballistic tests on 6061 aluminum reinforced by Al_2O_3 and SiC particles, with projectiles at velocities between 475 and 850 m/s. From that study, at a projectile velocity of 850 m/s, the reported penetration depth into a composite containing 30 vol.% Al_2O_3 particles was only half that into the unreinforced 6061 alloy. Better understanding of the constitutive response of similar metal–matrix composites at high rates of loading will lead to materials design and optimization schemes for ballistic applications. A review of the recent literature on the rate-dependent mechanical behavior of particle-reinforced metal–matrix composites is presented by Li and Ramesh [3]. Much of the literature involves studies of dynamic response in compression (e.g. [4]). There is a limited amount of work on the dynamic response in tension (e.g. [5–8]), and on the dynamic fracture of MMCs (e.g. [9,10]). However, the response to shearing is typically the dominant response function during the plastic deformations of ductile materials, and so multiaxial models for metal–matrix composite behavior typically make some assumptions on the shearing response. However, there has been essentially no work on the dynamic shearing response of such materials since the early work of Marchand et al. [11]. In pursuit of the objective of experimentally-verified multiaxial constitutive models for metal–matrix composites that are subjected to impact loads, this paper examines the dynamic shearing response of a metal–matrix composite and its associated metal matrix.

* Corresponding author. Tel.: +1 410 516 7735; fax: +1 410 516 7254.
E-mail address: ramesh@jhu.edu (K.T. Ramesh).
[1] Present address: Department of Aircraft Engineering, Northwestern Polytechnical University, Xi'an, P.R. China.

0921-5093/$ – see front matter © 2004 Elsevier B.V. All rights reserved.
doi:10.1016/j.msea.2004.04.062

Report Documentation Page

Form Approved
OMB No. 0704-0188

1. REPORT DATE	2. REPORT TYPE	3. DATES COVERED
17 APR 2004	**N/A**	**-**

4. TITLE AND SUBTITLE	5a. CONTRACT NUMBER
The Mechanical Response of an A359/SiCp MMC and the A359 Aluminum Matrix to Dynamic Shearing Deformations	5b. GRANT NUMBER
	5c. PROGRAM ELEMENT NUMBER
6. AUTHOR(S)	5d. PROJECT NUMBER
	5e. TASK NUMBER
	5f. WORK UNIT NUMBER
7. PERFORMING ORGANIZATION NAME(S) AND ADDRESS(ES) **Oak Ridge National Laboratory Bethel Valley Rd PO Box 2008 Oak Ridge, TN 37831-6063**	8. PERFORMING ORGANIZATION REPORT NUMBER
9. SPONSORING/MONITORING AGENCY NAME(S) AND ADDRESS(ES)	10. SPONSOR/MONITOR'S ACRONYM(S)
	11. SPONSOR/MONITOR'S REPORT NUMBER(S)

12. DISTRIBUTION/AVAILABILITY STATEMENT
Approved for public release, distribution unlimited

13. SUPPLEMENTARY NOTES

14. ABSTRACT

15. SUBJECT TERMS

16. SECURITY CLASSIFICATION OF:			17. LIMITATION OF ABSTRACT	18. NUMBER OF PAGES	19a. NAME OF RESPONSIBLE PERSON
a. REPORT	b. ABSTRACT	c. THIS PAGE			
unclassified	**unclassified**	**unclassified**	**UU**	**9**	

2. Materials

The materials investigated in this study are an A359 aluminum alloy and a MMC of the same alloy reinforced with 20 vol.% SiC particles. The A359 aluminum alloy was obtained from Alcan International Limited in the form of a cast bar 1.5 in. in diameter. The composition of the A359 aluminum alloy is (wt.%): 0.2 Cu, 0.5–0.7 Mg, 0.1 Mn, 8.5–9.5 Si, 0.20 Fe, 0.10 Zn, 0.20 Ti, 0.20 other, with the balance being aluminum. The composite was also obtained in the form of a cast bar 1.5 in. in diameter. Optical micrographs of the as-cast unreinforced alloy and of the as-cast composite are presented in Fig. 1a and b, respectively. The unreinforced alloy shows a classic as-cast eutectic microstructure with an interdendritic aluminum–silicon region containing fine silicon particles. The composite shows that the reinforcing silicon carbide particles are generally distributed along the eutectic phase with the finer silicon particles. The SiC particles are faceted with a slight preferred orientation. Microscopic quantitative analysis was conducted to determine the statistical characteristics of the reinforcement (Li et al. [4,12]). The mean SiC particle size in both the axial and the transverse sections of the as cast bar, is in the range of 6–18 μm with aspect ratios between 1.5 and 2.5. Vickers microhardness measurements were made in the unreinforced alloy and in the matrix of the composite. The load was chosen so that the longest length of the indentation in the matrix was less than half the distance to the nearest particle. The results are shown in Table 1. The data indicate that the hardness of the matrix material is very similar to that of the unreinforced alloy. The hardness results along with the similarity of the microstructures exhibited support the notion that the rate-dependent properties of the unreinforced alloy is comparable to the properties of the matrix in the composite for the purpose of analytical modeling.

Table 1
Comparison of Vickers microhardness and yield strength of the unreinforced alloy and the matrix of the composite material

Material	Mean diagonal (μm)	Vickers microhardness (kg/mm^2)	Yield strength (MPa)
A359 Al alloy	35.0 ± 0.4	75.6	252
A359/SiC composite	34.5 ± 0.8	78.0	260

Table 2
Measured failure strains in shear of the A359/SiC composite and the A359 alloy at various shear strain rates

Materials	Specimen #	Strain rate (s^{-1})	Failure strain (shear)	Equivalent failure strain in tension
A359 alloy	A359-1	710	0.184	0.106
	A359-2	760	0.213	0.123
	A359-3	1600	0.265	0.153
A359/SiC Composite	SiC-1	260	0.061	0.035
	SiC-2	920	0.073	0.042
	SiC-3	1420	0.114	0.066

The quasi-static and high-strain rates properties of these materials have been presented in compression [4], and tensile stress–strain curves for both the A359 alloy and the A359/SiC composite behavior are presented in Fig. 2 for (a) quasistatic and (b) high-strain-rate loading. The tensile failure strains reported by Li et al. [7] are summarized in Table 2. Substantial SiC particle fracture was observed in the composite subjected to compression loading [12]. In contrast, the tensile failures of both the A359 alloy and the A359/SiC

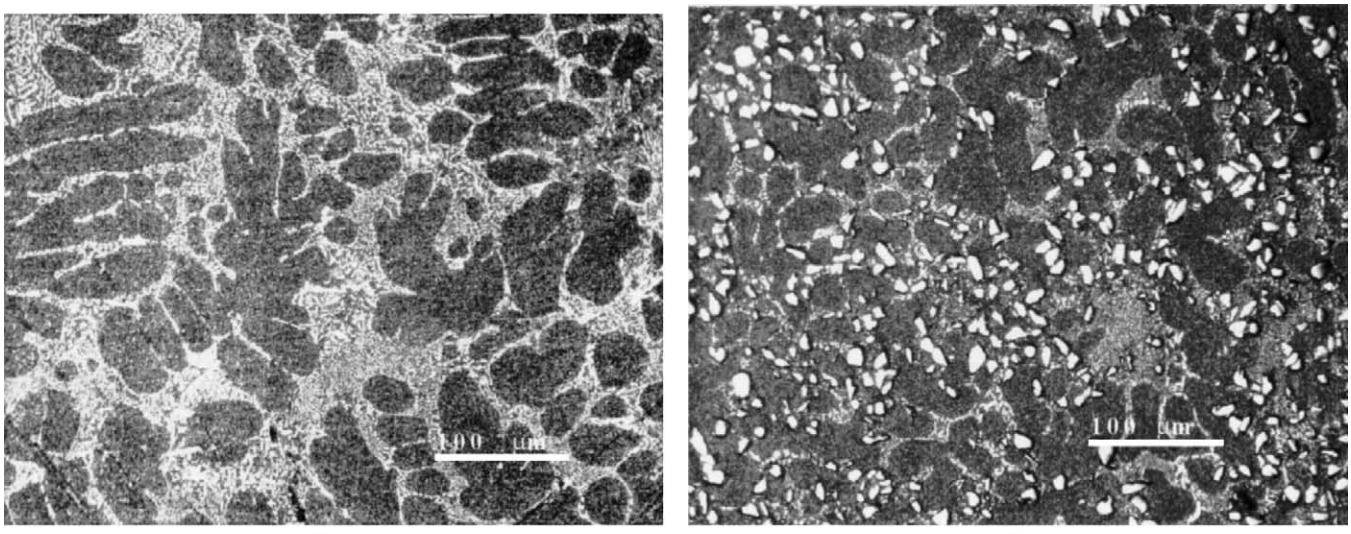

(a) (b)

Fig. 1. Optical micrographs of (a) as-received A359 alloy and (b) the as-received F3S.20S metal–matrix composite (A359 containing 20 vol.% SiC particles).

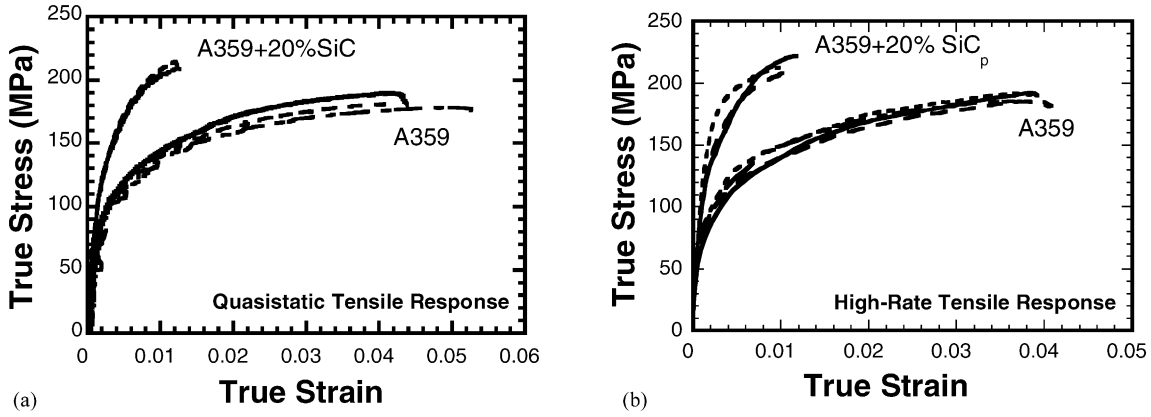

Fig. 2. Stress–strain curves of both composite and monolithic alloy in simple tension [7]: (a) quasistatic rates of deformation ($10^{-3}\,s^{-1}$); (b) high strain rates ($200\,s^{-1}$).

composite are dominated by fracture along the interdendritic aluminum–silicon eutectic region visible in Fig. 1, with no indication of SiC particle fracture [10]. These specific differences highlight the importance of relevant stress state in determining the damage mode and the effective constitutive response in MMCs. In this effort, we characterize the torsional response and the damage mode associated with the shearing stress state in these MMCs.

3. Experimental techniques

The primary approach to the measurement of high-rate shearing response is via the torsional Kolsky bar, first developed by Baker and Yew [13]. This method has been used to characterize the response of many metallic materials to high shear rates [14–19]. The torsion Kolsky bar technique has some advantages over the compression [4] and tension [7] Kolsky bar approaches for the investigation of high-rate constitutive behavior. First, the shearing mode eliminates the occurrence of necking, which needs to be accounted for in the tension Kolsky bar test, and the problem of barreling, which occurs in the compression Kolsky bar test when large strains are developed. Second, radial expansion and contraction are not significant in torsion of isotropic materials, so that the inertial and end effects present in the tension and compression tests are absent in the torsional Kolsky bar experiment. Finally, there is no dispersion of the torsional wave propagating in the elastic bars in the primary mode, so that the interpretation of the experimental results is more direct.

The axial/torsion Kolsky bar [20] operated in pure torsion mode is used to conduct all of the experiments described here. Two long elastic bars (see Fig. 3) are used as waveguides for the propagation of torsional waves, which do not show dispersion in the primary mode. The bar that carries the loading pulley is called the input bar, and the second bar is referred to as the output bar. The two bars are made of 7075-T651 aluminum and are each 1 inch in diameter. The actuators, bars and specimen are supported on an alignment table with specially designed bearing blocks. Strain gages are mounted on both bars (two on the input bar and one on the output bar) for measuring the shear strains in the bars. The specimen (the design of which will be presented in the next subsection) is attached between the two bars (typically using Epoxi-Patch 1105 high peel, supplied by Hysol Aerospace & Industrial Productions Division, cured for 18 h at room temperature).

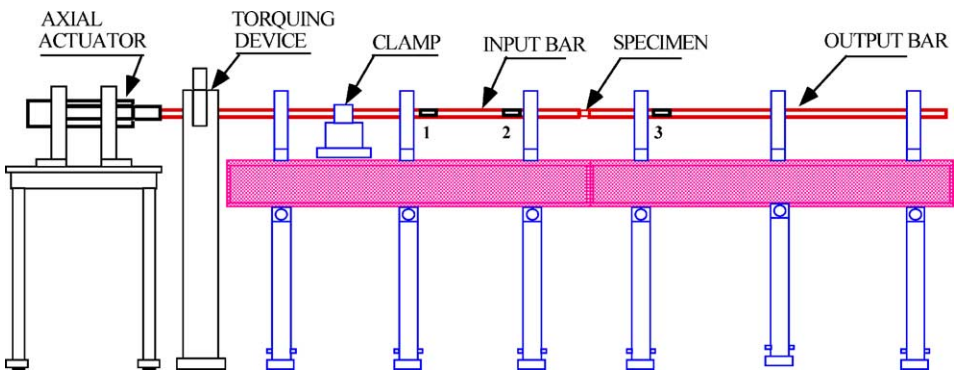

Fig. 3. Schematic diagram of the axial/torsional Kolsky bar, used in pure torsion mode.

To initiate the test procedure, a torque is applied to the short section of the input bar using a hydraulic system that drives the pulley while the rest of the bar is restrained using a friction clamp. The yield strength of the 7075-T6 aluminum limits the maximum stored input torque at 400 Nm. The friction clamp uses a notched bolt made of 2024-T4. This clamp is released by controlled breakage of the pre-notched bolt by a separate hydraulic system. This action results in a torsional pulse that propagates down the bar towards the specimen. The pulse amplitude is half the corresponding stored stress and the pulse duration is determined by the length of the bar between the loading device and the clamp. When the loading pulse reaches the specimen, part of it is reflected back into the input bar and part is transmitted through the specimen into the output bar. After several reverberations of the wave in the specimen, the shear stress in the specimen becomes nominally uniform, and the specimen deforms plastically under the applied load. The strain gages in the input and output bars are used to monitor the input pulse, reflected pulse and transmitted pulse, which are used to determined the strain rate, strain and stress in the specimen [20].

4. Torsional specimens

Specimens for torsional Kolsky bar tests are traditionally flanged thin-walled tubes. The flanges provide mechanical coupling between the bars and the specimen. Various forms of flange including hexagonal ends and right cylindrical ends have been used [21]. Similar specimen designs were used to characterize adiabatic shear band development in metals [18]. To assure stress uniformity across the wall thickness, the specimens are normally designed with $r_i/w \geq 25$ and $w \leq 0.5$ mm (where r_i is the inner radius and w is the wall thickness of the thin-walled tube specimen). The flanges are normally much larger than r_i to enable efficient load transfer without yielding. Fillet radii are applied at the flange to gauge-length transition region to avoid premature failure. These traditional torsional Kolsky bar specimen designs are very reliable, but have three significant drawbacks. First, a sizable blank larger than the diameter of the flanges is needed to machine out each specimen. This is a challenge in studying novel materials not in production, when only limited size and quantity of the material is available. This is also an issue with materials of low machinability (as is often the case with advanced composites). Second, because the wall thickness is so small while the rest of the specimen is so large, machining these specimens require great precision and time which result in the high cost. Third, it is extremely difficult to machine uniform thicknesses in such specimens. Although reaming (for the inner diameter) and centerless grinding can be used, these tend to develop circumferential thickness defects that are particularly deleterious and sensitive to large shear strains.

The specimen design applied in this paper addresses the aforementioned short comings of the traditional torsional Kolsky bar specimen. This new design is particularly suitable for the materials of interest in this paper. MMCs are difficult to machine and only small quantities of material are available from a single processed batch. Only single batch materials are considered in this study to avoid batch-to-batch variation that can statistically corrupt the experimental results. The resulting specimen design consists of several components that are then assembled to form the final specimen: two bases, two rings, a thin-walled tube and four small screws (see Fig. 4). The thin-walled tube in the specimen assembly is the material under investigation. The tube has an inner diameter of 15.25 mm, a wall thickness less than 0.5 mm, and a ratio of inner radius to wall thickness $r_i/w \geq 30.5$. The bases and the rings are made from steel using conventional machining, and are designed to couple the thin-walled tube specimen to the Kolsky bar for load transfer. The base diameter is identical to that of the Kolsky bar, and the diameter of the stepped portion is 25 μm less than the inner diameter of the thin-walled tube specimen. The step height is approximately 3 mm. The rings are 3 mm thick, with an inner diameter of 16.50 mm (25 μm larger than the outer diameter of the thin-walled tube), and an outer diameter equal to the outer diameter of the base. The screw holes are precision drilled to provide placement and alignment of the rings with respect to the base. The process of assembly is as follows: (1) the rings are aligned and screwed on to the bases with a thin layer of adhesive applied between the mating surfaces; (2) the annular gap between the base and the ring is then filled with the adhesive; (3) the thin-walled tube specimen is inserted into the gap with a small applied pressure that is held until the adhesive is fully cured (18 h). The resulting specimen assembly is now ready to be attached on to the Kolsky bars using the adhesive described earlier. In this study, the A359 and the A359/SiC composite tube specimens are produced by wire electric discharge machining (Wire EDM). The wall thickness of the tube specimen is approximately 500 μm. The wall thickness and roughness developed on the surface after EDM is much more uniform (in both the axial and circumferential directions) than that typically produced by centerless grinding, and thus the thickness defects prevalent in dynamic torsion

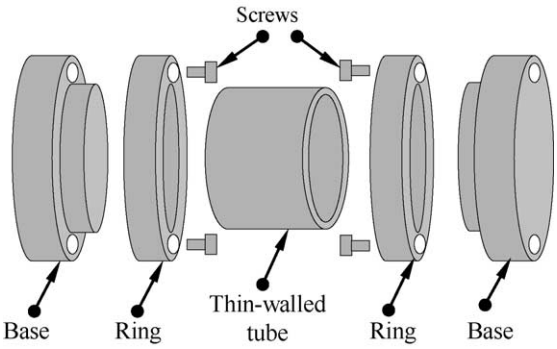

Fig. 4. Exploded schematic of the new specimen design. Note that the material under investigation is the material of the thin-walled tube.

tests of this test are minimized. This EDM process leaves a recast layer on the surface that is about 70 μm thick [22], which is comparable to the thickness of a plastically deformed layer from a grinding operation.

5. Results and discussion

5.1. Technique validation

Since the new torsional specimen design is more complex than the traditional torsional specimen, several experiments were performed to ensure that the new design provides an accurate measure of material behavior. The specimen assembly is designed to transfer the applied torque from the bar to the base, and then through the built-up ends into the thin-walled tube made of the material under investigation. Three concerns arise with this arrangement: First, is the adhesive sufficiently strong, or does slippage occur at any of the interfaces in this system (the bar-base interface and the base-ring-tube interfaces)? Second, is the adhesive a significant contributor to the apparent shear strain? Third, is torque equilibrium developed in the specimen early enough during the test to assure accurate representative of the bulk material behavior? The following sections address these concerns.

First, is the adhesive sufficiently strong, or does slippage occur at any of the interfaces in this system (the bar-base interface and the base-ring-tube interfaces)? Chichili and Ramesh [20] applied the same adhesive used in this study to investigate shear localization in α-titanium. The adhesive in that case sustained sufficient shear stresses between the bar and flange interfaces without slippage during testing. Since the A359 Al and the A359/SiC composite are of much lower strength than α-titanium, the adhesive should be suitable to transfer shear loading without slippage. This was confirmed by examinations of fiduciary lines on the specimen-tube assemblies after each test.

Second, is the adhesive a significant contributor to the apparent shear strain? This question stems from potential errors in the shear strain measurement arising from the elastic deformations of the adhesive in shear. The total thickness of the adhesive layer in the specimen assembly, including all interfaces, is limited to less than 100 μm. This ensures that the shear displacement contribution from the adhesive is negligible in comparison with that from the large plastic strains developed in the specimen.

Finally, the question of stress equilibration during the experiment is addressed by comparing the torques computed from the three measured pulses on the two sides of the specimen. The result is presented in Fig. 5. It is apparent that stress equilibration has been achieved at a very early stage in the loading (note that the time required for a torsional wave to transit the specimen is only 5 μs).

Fiducial markers on the specimens demonstrate that the specimens are being subjected to simple shear deformations, and the plastic strains computed from the measured pulses

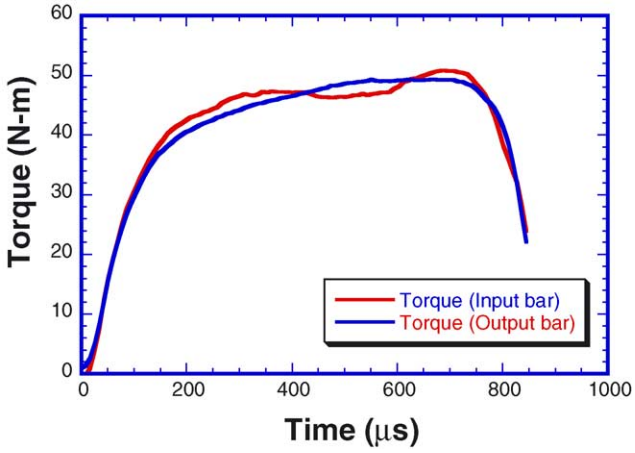

Fig. 5. Equilibration of torques. The torques at the specimen/input bar interface and the specimen/output-bar interface are shown.

are consistent with the strains estimated using the fiducial markers. All of the specimens fail through fracture of the thin-walled tube in the gauge length of the specimen rather than at the built-up ends. Put together, these observations demonstrate that the new specimen design is effective and does provide valid measures of the response of these materials under shear at high strain rates.

6. Experimental results

Fig. 6 presents shear stress versus shear strain curves for both the A359 unreinforced alloy and the A359/SiC metal–matrix composite. Considering first the response of the unreinforced A359 Al alloy, we see that fairly large shear strains (over 15%) are developed before failure of the specimen occurs (all of these experiments resulted in

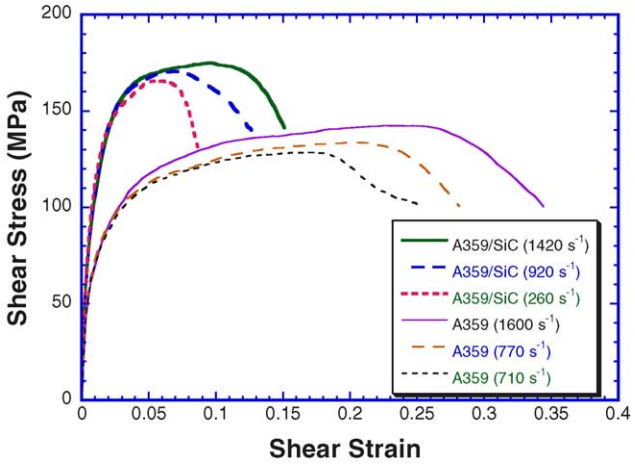

Fig. 6. Shear stress vs. shear strain curves obtained at various shear strain rates for both the unreinforced A359 alloy and the particle-reinforced A359/SiC metal–matrix composite. Note the substantial plastic deformations that are developed before failure.

specimen failure during the loading). The failure strain in torsion appears to increase with increasing shear rate. The flow stress appears to increase with increasing strain rate within the small range of strain rates presented in Fig. 6. The flow stress of this aluminum alloy has been shown to be rate-dependent when tested in compression [4], although the significant rate sensitivity observed in that work occurs at effective strain rates higher than those developed in the shearing deformations presented here (the strain rates attainable in these torsional tests are somewhat less than those attainable in high-rate compression). Thus the matrix behavior is typical of that expected from this metallic material.

Fig. 6 also shows that, as expected, the presence of the reinforcing particles results in a strengthening of the composite even in these torsional deformations. The A359/SiC composite exhibits flow stresses about 45% higher than the A359 matrix alloy in these torsion tests. Substantial plastic deformations (>5%) are developed in the composite prior to specimen failure in torsion, although the failure strains of the composite are of course smaller than those of the matrix material. Further, the degree of strain hardening observed from the composite stress–strain curves is similar to that exhibited by the particle-free A359 aluminum alloy. Several investigators [23–25] have shown that the strain hardening of a metal–matrix composite should be similar to that of the matrix at reasonably large strains (assuming no damage). These works along with the evidence of Fig. 6 and the SEM micrographs presented et seq suggest that particle fracture is not a dominant damage mechanism in shearing deformation of this composite. In contrast, a reduction in the strain hardening of this composite has been observed during compressive deformations as a result of particle fracture [12]. The development of damage mode is thus sensitive to the stress state.

The flow stress of the composite also appears to increase with strain rate following the apparent rate-dependent strengthening of the A359 Al matrix. The experimental results on rate-dependence presented here are consistent with the high-rate torsional experimental results from Marchand et al. [11] on 2124-T6 aluminum alloy reinforced by SiC whiskers. The presence of particulate reinforcements in a metal–matrix typically increases the strain rate sensitivity of the composite [3], in a manner which is strongly dependent on the reinforcement volume fraction, reinforcement shape and aspect ratio. Most observations of rate-hardening in metal–matrix composites have been in compression; it appears that the behavior in high-rate torsion is similar.

All the specimens of both the composite and monolithic alloy failed in torsion by fracture of the gauge section (i.e. within the thin-walled tube). By careful collection of the fragments from each test, we were able to reassemble the failed specimens. Typical photographs of the reassembled specimens are shown in Fig. 7a for the unreinforced alloy and in Fig. 7b for the metal–matrix composite. The fiduciary lines shown in Fig. 7a and b were initially parallel to the specimen axis. The post-mortem appearance of the fiduciary lines demonstrates the uniformity of the shear deformation. The failure process consists of cracks that propagated circumferentially around the specimen accompanied by occasional crack-branching. SEM micrographs of the fracture surfaces of the matrix and composite are presented in Fig. 8. Fractured particles are not a significant feature

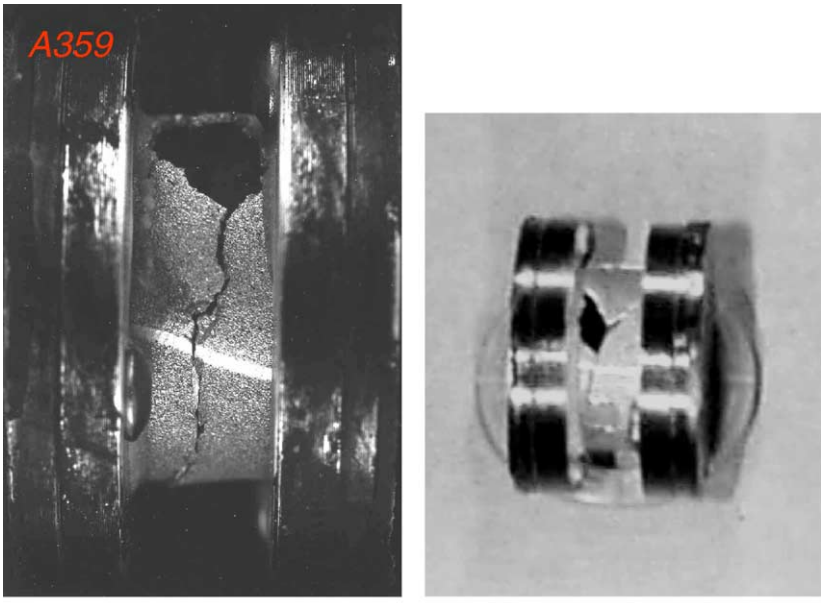

Fig. 7. Photographs of typical reassembled specimens after failure: (a) A359 alloy. Note the fiducial line, initially parallel to the specimen axis; (b) A359/SiCp metal–matrix composite. Failure occurs through the propagation of circumferential cracks.

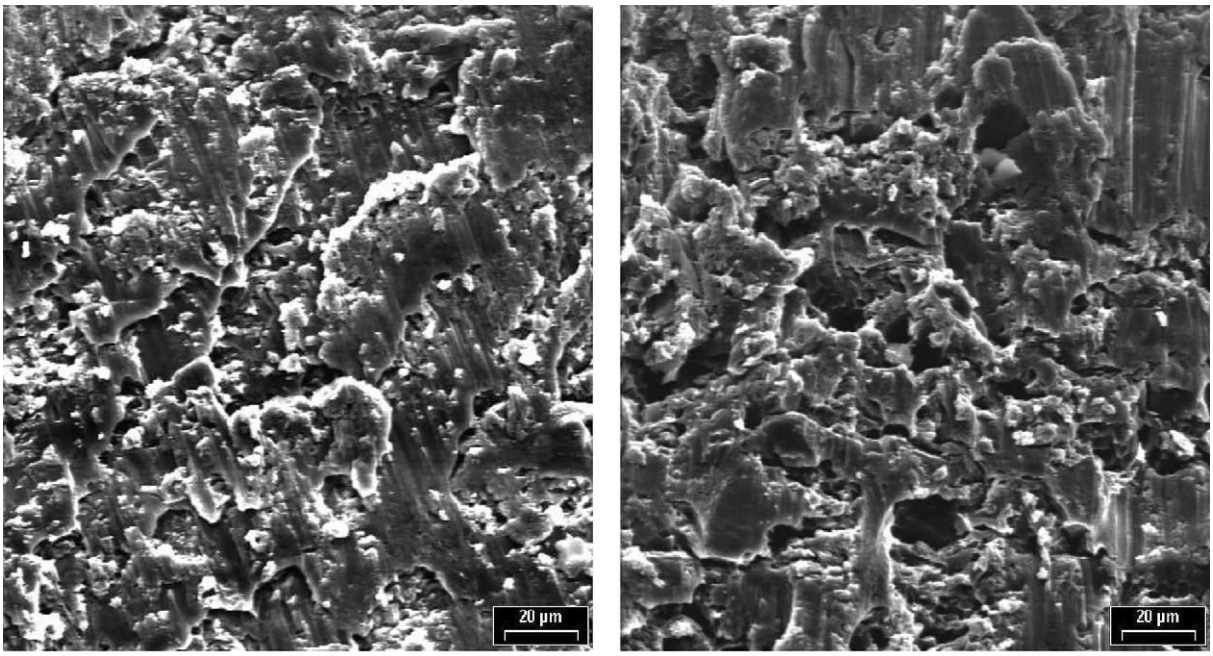

(a) (b)

Fig. 8. Fracture surfaces of (a) the matrix alloy and (b) the A359/SiCp metal–matrix composite after dynamic torsional deformations. Note in (a) the shear striations from the precipitates in the matrix, and in (b) fractured particles are not a significant feature of the composite fracture surface.

of the composite fracture surface, consistent with the lack of damage due to particle fracture during the deformations prior to macroscopic fracture.

It is well-known that the presence of ceramic particles increases the flow stress in the composite (Fig. 6), but also limits the failure strain of the material (typically through particle fracture or debonding at the particle-matrix interfaces). Though both A359 and A359/SiC have been shown to exhibit brittle behavior in tensile tests [7], these materials demonstrate relatively large plastic deformations in shear (Fig. 6). The failure strains from dynamic shear loading and their corresponding equivalent failure strains in tension are presented in Table 2. Comparison of the tensile strain to failure calculated from the torsion test data (Table 2) with that directly from tension tests (Table 3) shows substantially more effective ductility from shear than in tension. This behavior supports the ballistic experimental observations reported by Bless et al. [1] and Vaziri et al. [2]. The effect of the rate of loading on the failure strain is also of interest. In this study, the torsional failure strains increase at higher strain rates for both the unreinforced alloy and for the metal–matrix composite, and similar behaviors have been reported by Harding et al. [5] and Marchand et al. [11]). Rate-dependence of the failure strain of the particle-free matrix alloy may be related to the rate-dependence of the failure strain in the composite. Recent experimental results from dynamic tension testing of the A359 and A359/SiC indicated either slightly negative or negligible strain rate effects on failure strain (see Table 3) [7]. It appears, therefore, that the rate-dependence of the failure strain of these composites may be a function of the stress-state. This also indicates that the damage mechanisms in this composite are different in tension and torsion.

Table 3
Failure strains of the A359/SiC composite and the A359 alloy in simple tension [7]

Material	Quasi-static	Dynamic
A359 Al (Alcan)	0.045 ± 0.005	0.0405 ± 0.003
F3S.20S (Alcan)	0.012 ± 0.001	0.0108 ± 0.001

A comparison of the dynamic response of the A359 matrix alloy and the particle-reinforced A359/SiC metal–matrix composite in tension and torsion is presented in Fig. 9. In order to make this comparison, all stresses and strains have been converted to effective stresses and effective strains at the effective strain rates listed in the Figure. The effective stress is defined as $\sqrt{1/2S : S}$, where $S = \sigma - 1/3(tr\sigma)I$ is the deviatoric stress tensor, and the effective strain is the corresponding work-conjugate strain measure. Using this comparison (Fig. 9), one observes that the response of the matrix is similar in tension and torsion, although larger strains can be accommodated in shear (the slightly higher strength observed in torsion is likely the result of the higher effective strain rate in that test, combined with experimental scatter). Thus the response of the matrix material is consistent with the traditional J_2-flow model for metals. Typical models for metal–matrix composites assume such behavior for the matrix, and predict a similar macroscopic J_2-flow response for the plastic deformation of the composite when damage is

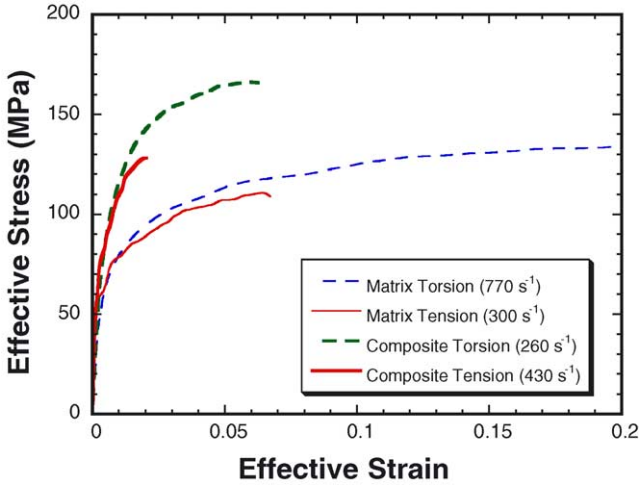

Fig. 9. Comparison of the dynamic response of the A359 matrix alloy and the particle-reinforced A359/SiC metal–matrix composite in tension and torsion. All stresses and strains plotted are effective stresses and effective strains, with the effective strain rates provided. Note that the response of the matrix is consistent with traditional J_2-flow models for metals, while the composite displays strong dependence of the response on the stress-state due to damage.

not included in the model [3]. However, Fig. 9 shows that the composite strength in tension is less than would be predicted by J_2-flow theory using the torsional data. The typical models for damage in metal–matrix composites assume that reinforcement particle fracture will occur in tension, but that is not the case in this material (where the tensile failures are observed to result from cracking along Si-rich paths). Thus multiaxial constitutive models for these metal–matrix composites must appropriately handle the dependence of the damage mechanism on the stress state. In subsequent work, we will seek the development of a physically validated multiaxial constitutive model for these materials that can correctly handle the effect of the stress state on the various active damage mechanisms.

7. Summary

We have developed and validated a new specimen design for torsional Kolsky bar experiments that simplifies the application of this technique for the study of advanced materials, such as metal–matrix composites, and allows the study of smaller quantities of materials available only in limited forms. This technique was applied to the study the dynamic response of an A359 aluminum alloy and of an A359/SiC_p metal–matrix composite in shear. The following highlights result from this study:

- The new specimen design can be effectively used for such hard-to-machine materials. The design not only substantially reduces the cost of machining, but also attains a more uniform distribution of stress and strain in the specimen than the traditional specimen. The effect of defects caused by the machining on the failure strain can be greatly reduced, and so these specimens may be useful in the investigation of adiabatic shear bands.
- Shear stress versus shear strain curves have been obtained on both the unreinforced aluminum alloy and the metal–matrix composite from high-rate shear deformations. The composite is significantly stronger than the matrix alloy in shear, and retains the same strain hardening characteristics as the matrix alloy (indicating that particle fracture does *not* occur in shear, unlike in compression).
- The failure strains in shear of both the composite and the unreinforced alloy increase with increasing shear strain rate. The ductility of both materials is greater in shear than in simple tension.
- The response of the metal–matrix composite in shear cannot be obtained using the tensile response together with J_2-flow theory, although the flow stress of the matrix alloy can be effectively described using this traditional approach for metals.

Acknowledgements

This work was supported by the US Army Research Office under Grant No. DAAH04-95-2-0006 and by the US Army Research Laboratory through Grant Nos. DAAL01-96-2-0047 and under ARMAC-RTP Cooperative Agreement Number DAAD19-01-2-0003. The authors wish to acknowledge useful discussions with K.J. Hemker of Johns Hopkins, and to express appreciation for the assistance of D. Olson and S. Martin in specimen preparation. Last but not least, the authors would like to thank Dr. D. Doutre of Alcan International Ltd. for supplying us with both the unreinforced alloy and the composite material.

References

[1] S.J. Bless, D.L. Jurick, S.P. Timothy, M.A. Reynolds, in: M.A. Meyers, L.E. Murr, K.P. Staudhammer (Eds.), Shock-Wave and High-Strain-Rate Phenomena in Materials, Marcel-Dekker, New York, 1992, p. 1051.
[2] R. Vaziri, D. Delfosse, G. Pageau, A. Poursartip, Int. J. Impact Eng. 13 (1993) 329.
[3] Y. Li, K.T. Ramesh, Acta Mater. 46 (1998) 5633.
[4] Y. Li, K.T. Ramesh, E.S.C. Chin, Int. J. Solids Struct. 37 (2000) 7547.
[5] J. Harding, B. Derby, S.M. Pickard, M. Taya, in: F.L. Matthews, N.C.R. Buskell, J.M. Hodgkinson, J. Morton (Eds.), Proceedings of the Sixth International Conference on Composite Materials (ICCM VI), vol. 3, Elsevier, London, 1987, p. 76.
[6] D.R. Chichili, K.T. Ramesh, Int. J. Solids Struct. 32 (1995) 2609.
[7] Y. Li, K.T. Ramesh, E.S.C. Chin, 2004, in press.
[8] Y. Li, K.T. Ramesh, E.S.C. Chin, Mater. Sci. Eng. A 371 (2004) 359.
[9] K. Cho, S. Lee, Y.W. Chang, J. Duffy, Metall. Trans. A 22A (1991) 367.
[10] Y. Li, K.T. Ramesh, E.S.C. Chin, Key Eng. Mater. 243–244 (2002) 57.

[11] A. Marchand, J. Duffy, T.A. Christman, S. Suresh, Eng. Fracture Mech. 30 (1988) 295.
[12] Y. Li, K.T. Ramesh, E.S.C. Chin, Acta Mater. 48 (2000) 1563.
[13] W.E. Baker, C.H. Yew, Trans. ASME J. Appl. Mech. 33 (1966) 917.
[14] J. Duffy, J.D. Campbell, R.H. Hawley, Trans. ASME J. Appl. Mech. 38 (1971) 83.
[15] J.L. Lewis, J.D. Campbell, Exp. Mech. 12 (1972) 520.
[16] A.M. Eleiche, J. Duffy, Int. J. Mech. Sci. 17 (1975) 85.
[17] J. Lipkin, J.D. Campbell, J.D. Swearengen, J. Mech. Phys. Solids 26 (1978) 251.
[18] A. Marchand, J. Duffy, J. Mech. Phys. Solids. 36 (1988) 251.
[19] K.T. Ramesh, S. Yadav, J.A. Davis, in: A. Bose, R.J. Dowding (Eds.), Tungsten and Tungsten Alloys 1992, Metal Powder Industries Federation, Princeton, NJ, 1993, p. 299.
[20] D.R. Chichili, K.T. Ramesh, J. Appl. Mech. 66 (1999) 10.
[21] K.T. Ramesh, Mech. Mater. 17 (1994) 165.
[22] G. Semon, A Practical Guide to Electro-Discharge Machining, Ateliers des Charmilles S.A., 1975.
[23] A.G. Evans, J.W. Hutchinson, R.M. McMeeking, Scripta Metall. Mater. 25 (1991) 3.
[24] J. Llorca, A. Needleman, S. Suresh, Acta Metall. Mater. 39 (1991) 2317.
[25] G. Bao, J.W. Hutchinson, R.M. McMeeking, Acta Metall. Mater. 39 (1991) 1871.